An analytical model for beach erosion downdrift of groins: Case study of Jeongdongjin Beach, Korea

Changbin Lim[1], Soonmi Hwang[2], Jung Lyul Lee[3]

[1]School of Civil, Architecture and Environmental System Engineering, Sungkyunkwan University, 2066, Seobu-ro, Suwon 16419, Korea
[2]Department of Coastal Management, GeoSystem Research Corporation, 172 LS-ro, Gunpo 15807, Korea
[3]Graduate School of Water Resources, Sungkyunkwan University, 2066, Seobu-ro, Suwon 16419, Korea

Correspondence to: Jung Lyul Lee (jllee6359@hanmail.net)

Abstract.

Beach erosion at the unprotected downdrift end of a groin is common, when waves approaching obliquely to the structure. This phenomenon, has often occurred at downdrift of natural groins on the east coast of South Korea during high waves in winter months. The resulting planform assumes a distinctive crenulate shape with a maximum indentation point landward of the erosion. An analytical model is employed to study the beach erosion at the downdrift end of a natural rock groin at Jeongdongjin Beach in Korea, using mathematical equations derived from the parabolic model for headland-bay beaches in static equilibrium, to predict the downdrift control point and maximum indentation of the eroded shoreline. These equations are solves using the prevailing wave height, wave angle at breaking and wave direction derived from analysing NOAA's wave data over 40 years, and the longshore sediment transport rate calculated from the wave data. Location of the calculated maximum indentation is also verified using shoreline video monitoring data and compared with the result of one-line numerical model for shoreline change. Limitation of the proposed analytical model is discussed, as well as the effect of sediment bypassing the groin.

Keywords: Parabolic model, Downdrift erosion, Oblique wave incidence, Maximum indentation point, Shoreline video monitoring.

1 Introduction

Although seawalls of vertical or sloping (revetments) have been used for many decades as a purported protection in an erosive situation, it is however unfortunate that they have often promoted further erosion, not only to the beach in front of them but also at downdrift, where a seaward-concave planform is produced (Kraus and McDougal, 1996). On the other hand, groins of moderate dimension running from the beach into the sea at right angles or inclined have also produced unwanted beach erosion, despite they were installed to intercept/accumulate sediment on the updrift side. This type of beach erosion at the downdrift end of a shore-based coastal structures (e.g., seawalls, revetments and groins), which is known as beach flanking, is common,

yet rarely being taught in the classrooms nor well documented in the literature. It results in a localized eroding beach in crenulate shape. In the case of groins, whilst the sediment being accreted, their downdrift beach that suffers erosion can only recover after the updrift shoreline has built up to the tip (head) of the structures, after sediment bypassing occurs.

On the east coast of Korea (Fig. 1), low waves from ENE direction prevail in summer and high waves from NE dominate in winter. This causes seasonal change of shoreline orientation (Kim and Lee, 2015), as well as localized beach erosion up to 30 m at downdrift of some natural groins due to high waves in the winter months. For example, severe erosion with maximum retreat about 40 m was once observed (Fig. 2b) during February to March in 2016 at updrift side of Jeongdongjin Beach (129º02'26" E, 37º41'37" N; Fig. 1) in Gangwon-do (i.e., Province), where oblique high waves in winter encountered a cluster of natural pillar rocks protruding about 80 m into the open sea. Rail-bike (pedal-powered rail-cycles) tracks and the inner wall of Hourglass Park were damaged (Fig. 3).

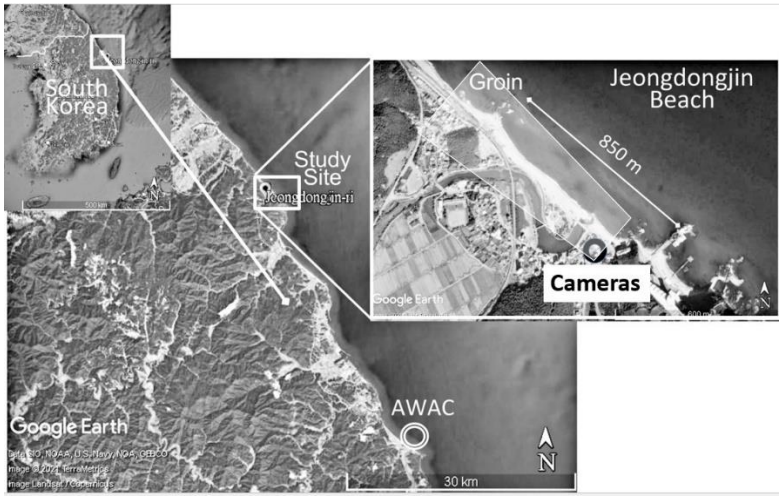

Figure 1: Location of Jeongdongjin Beach in Gangwon-do on the east coast of South Korea © Google Earth.

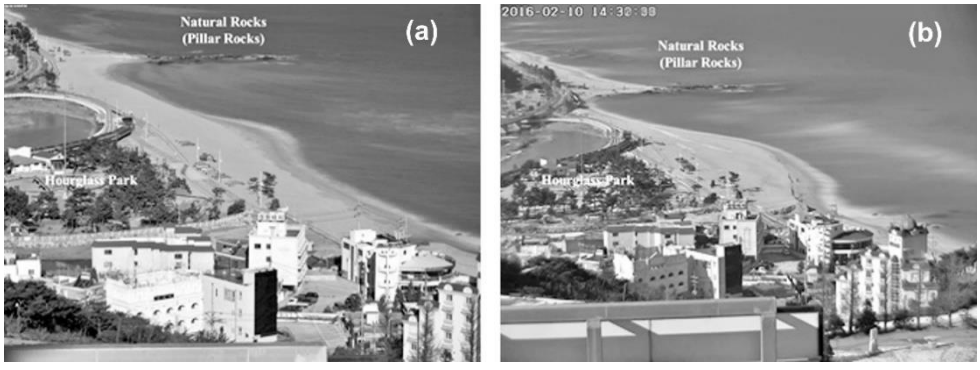

Figure 2: Beach erosion at Jeongdongjin Beach, South Korea caused by (a) low waves on 04 December 2015 and (b) high waves on 10 February 2016.

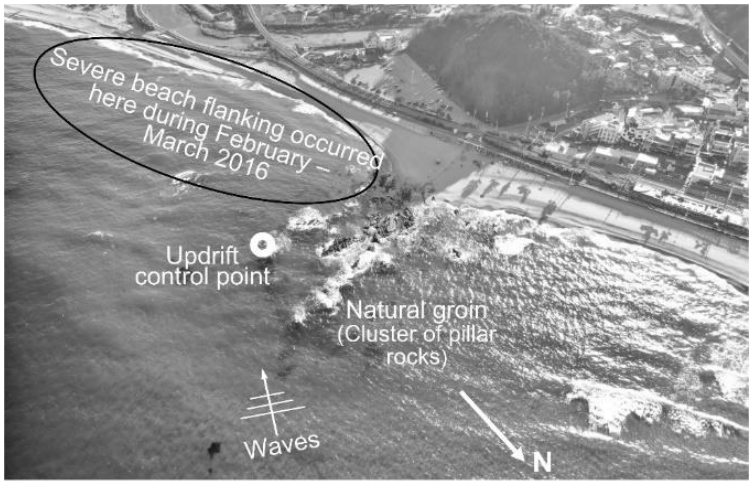

Figure 3: Location of pillar rocks seaward of Jeongdongjin Beach, where downdrift erosion had occurred.

Beach erosion at downdrift of groins and their negative impact have been well studied theoretically or in prototype (Lehnfelt and Svendsen, 1958; Bakker, 1968, Bakker et al., 1970; Price and Tomlinson, 1970; Magoon and Edge, 1978; Headland et al., 2000; USACE, 2002). To investigate the effect of groins on beach erosion, Badei (1995) conducted laboratory experiments to reproduce the shoreline planform and topographic changes, while Wang and Kraus (2004) performed tests on erosion without longshore sediment transport (LST). Numerical approach has also been used. For example, Pelnard-Considère (1956) proposed a one-line model that can simulate the temporal changes of the shoreline associated with groins. The applicability of this model has been verified in various situations by applying the concept of longshore diffusivity (e.g., Le Méhauté and Soldate, 1979; Walton and Chiu, 1979; Larson et al., 1987). Among them, Ozasa and Brampton (1980) developed a beach topography change model that can simulate a crenulate shape due to wave diffraction. Hanson and Kraus (1989) produced the GENESIS model for calculating long-term shoreline changes, while Leont'yev (1997) proposed a short-term shoreline change model. However, most of these have not specifically reported the magnitude of downdrift erosion caused by oblique waves to a groin.

The long-term stability of shoreline depends on the balance between the LST and sediment characteristics at wave breaking (Longuet-Higgins, 1970; Komar and Inman, 1970; USACE, 1984; Kamphuis, 1991; Bayram et al., 2007). Because a new shoreline planform induced by downdrift erosion may reach stable condition, it is imperative to assess its equilibrium status using an appropriate model, empirical and/or numerical (Balaji et al., 2017). Among the empirical models available for embayed beaches, which include logarithmic spiral (Krumbein, 1944; Yasso, 1965), parabolic bay shape model (PBSE; Hsu and Evans, 1989) and hyperbolic tangent model (Moreno and Kraus 1999), only the parabolic model is derived for the static equilibrium planform (SEP). When a SEP is reached, LST is not required to maintain the shoreline stability, because waves would break simultaneously along the bay periphery (Hsu et al., 2000). Nowadays, together with the equilibrium beach profile, the concept of equilibrium beach that incorporates the parabolic model for shoreline planform has been widely used in

engineering design for beach nourishment projects (González et al., 2010), as well as a means for project planning (USACE, 2002). Recently, Lim et al. (2019) have also confirmed the validity of the parabolic model using wave data from the east coast of South Korea, to estimate the impact of engineering structures (e.g., jetties and groins). Moreover, Lim et al. (2021) have also demonstrated the effect of wave diffraction caused by coastal structures, supported by numerical models (e.g., Xbeach and Sbeach) that include waves, currents and topographic changes.

The aims of this paper are threefold, (1) to derive mathematical equations for calculating the position of the maximum indentation in the eroded beach, (2) to demonstrate the applicability of an analytical model derived from the parabolic model, and (3) to apply the mathematical equation to downdrift erosion at Jeongdongjin in Korea. These equations are solved using the prevailing wave conditions and the LST in winter months at Jeongdongjin which are obtained from analyzing NOAA's wave data. In this paper, a brief introduction is first given in section 1, while section 2 describes the analytical model using the parabolic model and the derivation of mathematical equations for the downdrift control point and the maximum indentation on the eroded beach. Analysis of NOAA's wave data over 40 years is presented in section 3.1 which provides averaged wave heights and wave angles at breaking for solving the mathematical equations (sections 2.2 and 2.3) and the seasonal LST rate (section 3.2) for one-line shoreline change model outlined in section 4. The analytical results for the maximum indentation point are then compared with the results of the numerical model and that from shoreline video monitoring project at Jeongdongjin Beach (section 4). Finally, discussions on the limitation of the proposed analytical model and the effect of sediment bypassing are given in section 5. Concluding remark is given in section 6.

2. Methodology

2.1 Parabolic bay shape model

This empirical model is based on the parabolic bay shape equation (PBSE; Hsu and Evans, 1989) that defines the location of a point $P(\theta, R)$ on an embayed beach in static equilibrium (SEP) by

$$R(\theta) = \frac{a}{\sin\beta}\left[C_0 + C_1\left(\frac{\beta}{\theta}\right) + C_2\left(\frac{\beta}{\theta}\right)^2\right] \quad \text{for } \theta \geq \beta \tag{1a}$$

$$R(\theta) = \frac{a}{\sin\beta} \quad \text{for } \theta \leq \beta \tag{1b}$$

As shown in Fig. 4, R denotes the radial distance from the parabolic focus (i.e., updrift control point) to a point (P) on the equilibrium shoreline; a is the distance between the wave crest base line at the focus and the tangent passing through the downdrift control point (Q) is parallel to the wave crest baseline; β is the angle between the wave crest baseline and the line joining the focus and point Q; θ is between the wave crest base line and the radius R. Coefficients C_0, C_1 and C_2 are the values

derived from regression analysis of 27 SEPs in mixed cases of laboratory and prototype data (Hsu and Evans, 1989). At point
95 Q, the boundary condition requires $C_0 + C_1 + C_2 = 1.0$ (unity) to ensure a common tangent at $\theta = \beta$.

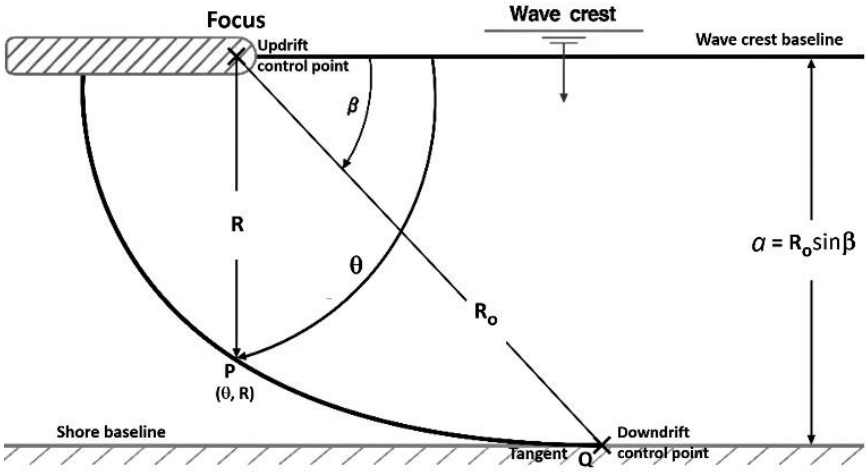

Figure 4: Definition sketch of parabolic bay shape model proposed by Hsu and Evans (1989).

When the downdrift straight section of an embayment is long, Eq. (1b) can be approximated as,

$$R(\theta) = \frac{\beta}{\sin\beta}\frac{a}{\theta} \tag{2}$$

100 If waves break at an angle α_b around the downdrift control point Q, then α_b can be expressed by Eq. (3) from the approximation of Eq. (2). In the absence of β in Eq. (3), θ can be solely determined from wave angle α_b at wave breaking, or vice versa,

$$\alpha_b(\theta) = \tan^{-1}\left(\frac{dy}{dx}\right) = \tan^{-1}\left(\frac{\sin\theta - \theta\cos\theta}{\cos\theta + \theta\sin\theta}\right) \tag{3}$$

The relationship between θ and α_b in Eq. (3) for a SEP can be readily calculated and expressed explicitly using figure or table.
105 For example, the three key values of α_b (= 10°, 20° and 30°) correspond to θ of 52.5°, 71.2° and 86.5°, respectively.

2.1.1 Downdrift control point

Consider a simple littoral cell without sediment supply from updrift side, in which shoreline and depth contour are initially straight and parallel, is subjected to oblique wave action and the LST is blocked within two groins, one short unit on the left-hand side and another long unit on the right-hand side (Fig. 5). Initially, beach erosion is minor, when the downdrift control
110 point (or transition point A) reaches one-sixth of the length between the groins, without wave diffraction (top panel in Fig. 5). Under longer duration of wave action, beach erosion at downdrift of a short groin increases and the control point A could be

extended downward reaching one-third of the length (*B*) between the groins. Crenulate bay shape is not developed, due to no wave diffraction. As wave action continues, the length of beach erosion expands with control point *C* reaching one-half of the beach length (lower panel in Fig. 5). In this figure, parameters $t_{1/6}$, $t_{1/3}$ and $t_{1/2}$ denote the time when the control point reaches 1/6, 1/3 and 1/2 of the beach length *L* between the groins, respectively. At $t \geq t_{1/2}$, planform will remain in equilibrium.

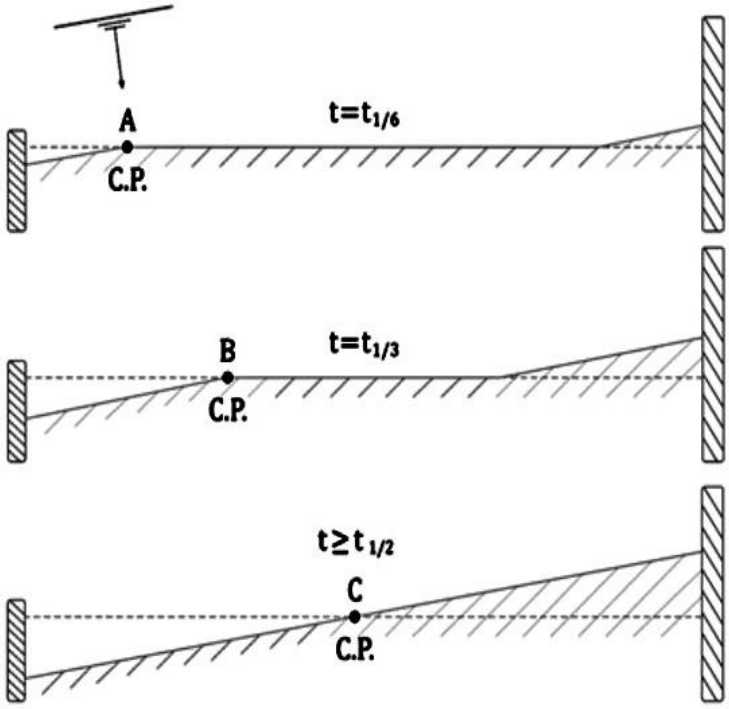

Figure 5: Temporal variations of downdrift control point due to oblique waves within a littoral cell.

In the case of short groin without bay shape formation, the position of the control point x_c, measured from the groin on the left-hand-side, can be expressed as a function of the elapsed time *t* and the LST rate Q_l (see Sect. 3.2). From the relationship of planar sediment area and beach geometry,

$$\frac{Q_l t}{(h_C+h_B)} = \frac{x_c^2 \tan\alpha_b}{2}, \tag{4a}$$

it renders

$$x_c = \sqrt{\frac{2Q_l t}{(h_C+h_B)\tan\alpha_b}} = \sqrt{\frac{2q_b \sin 2\alpha_b t}{\tan\alpha_b}} = 2\sqrt{q_b t}\cos\alpha_b = 2\,\eta\cos\alpha_b \tag{4b}$$

where the LST rate Q_l (unit: [m^3]) is given by $q_b \sin 2\alpha_b \times (h_c + h_B)$, in which α_b is the wave angle at breaking, q_b has the unit of m^2 and η (= $\sqrt{q_b t}$) has the unit of [m$\sqrt{t}$]. Equation (4) indicates the position of the control point is a function of LST rate, wave angle α_b at breaking and time ($\sqrt{t}$), from which the time elapsed for the control point to reach a distance of x_c can be rearranged as

$$t = \left(\frac{x_c}{2\sqrt{q_b}\cos\alpha_b}\right)^2 = \left(\frac{1}{2\cos\alpha_b}\right)^2 \tau \quad (5)$$

where τ is defined as x_c^2/q_b. When the eroded beach reaches SEP, $x_c = L/2$, where L = 850 m is the length of the shoreline between two groins (Fig. 1), and the time elapsed $t_{1/2}$ can be given by

$$t_{1/2} = \left(\frac{L}{4\sqrt{q_b}\cos\alpha_b}\right)^2 \quad (6)$$

Equation (6) implies that the time required to reach equilibrium increases as the LST decreases, but as beach length and wave obliquity increase. This approach can also be applied to a single littoral cell system affected by wave diffraction around a moderate or long groin with protruding length y_g, which is located at $\theta = \pi/2$ using the parallel shoreline assumption (see definition sketch of parabolic model in Fig. 4) of Hsu and Evans (1989). Hence, the shoreline advance width ($y_{\pi/2}$) of the parallel shoreline is expressed as

$$\frac{y_{\pi/2}}{y_g} \cong \frac{y_g - R(\pi/2)}{y_g} = 1 - \frac{2}{\pi}\frac{\beta}{\sin\beta} \quad (7)$$

where β is assumed to converge to zero, C_1 is unity, and C_0 and C_2 are zero.

2.1.2 Maximum indentation point

In Fig. 6, the cross mark '×' indicates the maximum indentation position on each of the beach erosion shape at different time steps. Here, the shoreline orientation at downdrift end is assumed to be the same as the wave breaking angle (α_b) for applying the parabolic model based on the downdrift control point (*A*, *B* and *C*, respectively, as in Fig. 6) at each time step. An example is illustrated in Fig. 7.

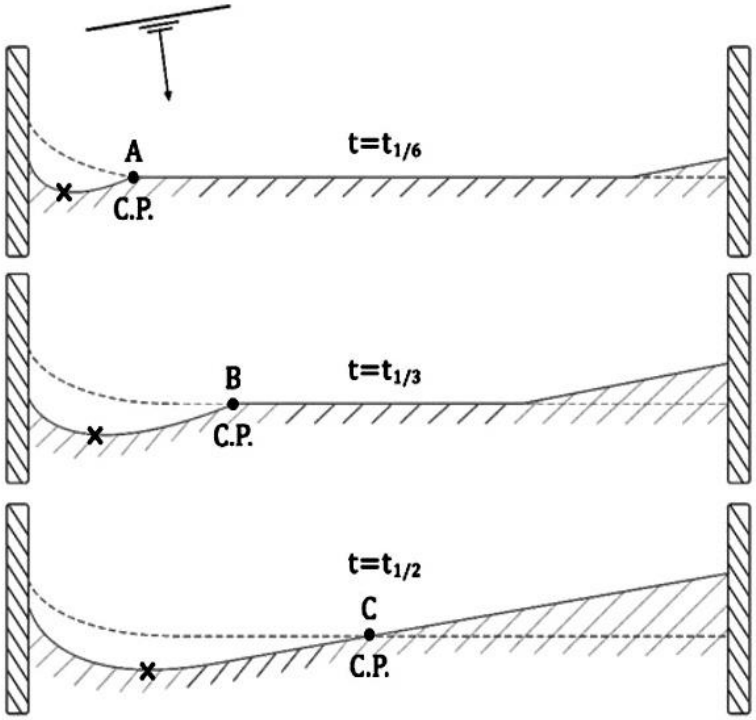

Figure 6: Temporal change of the downdrift control point (C.P.) for applying the parabolic model including the effect of wave diffraction due to oblique waves within a littoral cell, also showing maximum indentation (×) at each time step.

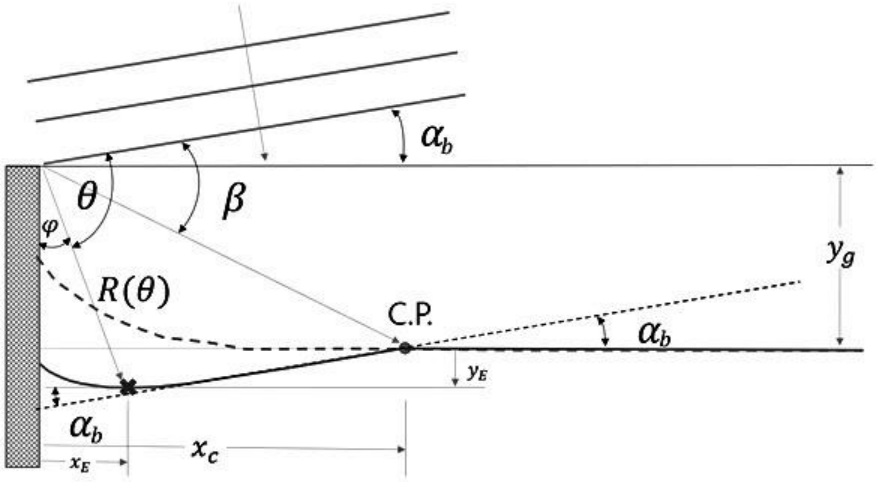

Figure 7: Application of the parabolic model based on the estimation of α_b and downdrift control point (C.P.) and wave diffraction at the downdrift of a groin.

The location of the maximum indentation point (x_E, y_E), shown in Fig. 7, can be determined using the PBSE approximation given by

$$x_E = R(\theta)\sin\varphi = R(\theta)\sin\left(\frac{\pi}{2} + \alpha_b - \theta\right) \tag{8a}$$

$$y_E = y_g - R(\theta)\cos\varphi = y_g - R(\theta)\cos\left(\frac{\pi}{2} + \alpha_b - \theta\right) \tag{8b}$$

where angle θ is for locating the maximum indentation given by Eq. (3) from the wave direction α_b at breaking. In addition, x_E is the distance measured from the groin in the direction of the initial (mean) shoreline, and $R(\theta)$ is a time-variant function of x_c, which can be obtained by Eq. (9) using the approximation of the parabolic model in Eq. (2),

$$R(\theta) \cong \frac{a}{\theta} = \frac{(y_g + x_c \tan\alpha_b)\cos\alpha_b}{\theta} \tag{9}$$

Applying Eq. (9) to Eqs. (8a) – (8b) results in an alternative expression for x_E and y_E,

$$x_E = \frac{(y_g \cos\alpha_b + x_c \sin\alpha_b)}{\theta}\sin(\varphi) \tag{10a}$$

$$y_E = y_g - \frac{(y_g \cos\alpha_b + x_c \sin\alpha_b)}{\theta}\cos(\varphi) \tag{10b}$$

where $\varphi = \frac{\pi}{2} + \alpha_b - \theta$. Consequently, a linear relationship for x_E and y_E can be established,

$$y_E = y_g - \cot(\varphi)x_E \tag{11}$$

Moreover, Eqs. (10a), (10b) and (11) can be non-dimensionalised using y_g, rendering

$$x_E' = \frac{(\cos\alpha_b + \eta' \sin 2\alpha_b)}{\theta}\sin(\varphi) \tag{12a}$$

$$y_E' = 1 - \frac{(\cos\alpha_b + \eta' \sin 2\alpha_b)}{\theta}\cos(\varphi) \tag{12b}$$

$$y_E' = 1 - \cot(\varphi)x_E' \tag{13}$$

where $\eta' = \eta/y_g$. Figure 8 shows the locations of $x_E' = x_E/y_g$ and $y_E' = y_E/y_g$ as a function of dimensionless $\eta' = \eta/y_g$ (0 to 4 with increments of 1.0) and different values of α_b from 1 to 30°. This figure indicates that the erosion width y_E increases with the increase of several parameters (i.e., the protruding length of the groin y_g, q_b, t and α_b).

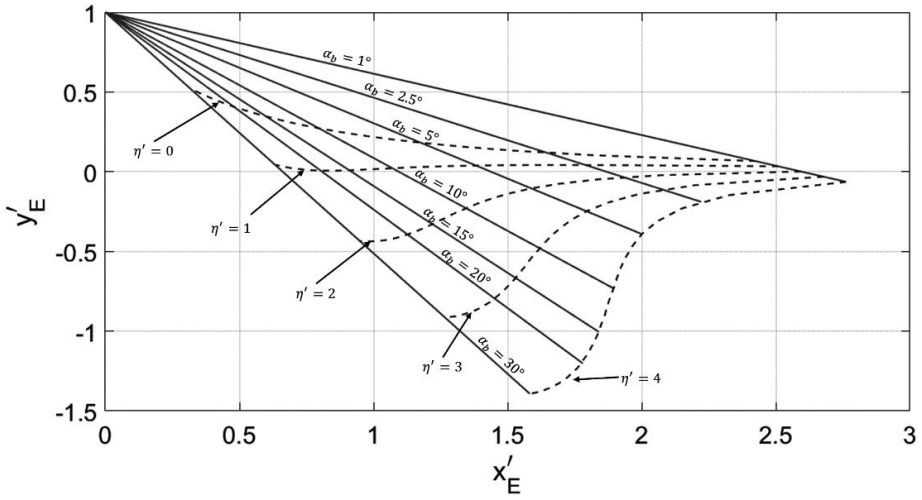

Figure 8: Location of $x_E{}' = x_E/y_g$ and $y_E{}' = y_E/y_g$ for maximum indentation point, based on the dimensionless variable $\eta' = \eta/y_g$.

2.2 Longshore sediment transport equation

Komar and Inman (1970) conducted field experiments on longshore energy flux, P_l, and longshore sediment transport (LST) rate, Q_l, expressing their relationship as

$$Q_l = CP_l = \frac{KP_l}{(\rho_s - \rho)(1-p)g} \tag{14}$$

where ρ, ρ_s, p and g are the seawater density, sediment density, sediment porosity (typically about 0.3 – 0.4) and acceleration due to gravity, respectively. I_l is the immersed weight of the sediment transport rate, K is a dimensionless coefficient (e.g., CERC coefficient) dependent on seabed property and significant wave height, which can be taken as 0.39 (Shore Protection Manual, 1984), but was taken as 0.77 in Komar and Inman (1970). The alongshore component of the energy flux per unit length of beach P_l is defined by

$$P_l = \left(EC_g\right)_b \cos\alpha_b \sin\alpha_b \tag{15}$$

where subscript b denotes the condition at wave breaking, $\left(EC_g\right)_b$ is the wave energy flux at breaking, and $\alpha_b$is the breaking wave angle between the shoreline and wave crest line. Equations. (14) and (15) can be combined and expressed as a function of wave height (H_b) and breaking wave direction (α_b),

$$Q_l = CH_b^{5/2} \sin 2\alpha_b \tag{16}$$

where the unit for Q_l is [m^3/s], $C\left(=\frac{K\sqrt{g/\kappa}}{16(s-1)(1-p)}\right)$ has a value of 0.0847 for most types of sand, in which K = 0.39, g = 9.81 m/s^2, spilling wave breaking index κ = 0.78, and sediment specific gravity s = 2.57 and porosity p = 0.35 for most types of sand.

The LST rate in Eq. (16) can be expressed using deep-water wave data shown in Eq. (17), assuming that the isobath of the seabed is parallel to the straight shoreline, resulting in

$$Q_l = C_{ol} H_O^{2.4} T_O^{0.2} \cos\alpha_O^{1.2} \sin\alpha_O \tag{17}$$

where C_{ol} is a constant, H_o and T_o are the significant wave height and wave period in deep water, respectively. The wave direction in the deep water α_O is measured between the outward normal to the shoreline and wave orthogonal or from the true north θ_O, as shown in Fig. 9, thus $\alpha_O = \frac{\pi}{2} - \theta_O - \beta$, with a positive amount of sediment pointing south and a negative pointing north. Furthermore, C_{ol} is a factor that reflects the characteristics of the sediment and waves, including specific gravity, porosity, breaking index and wave angle, rendering

$$C_{Ol} = \frac{Kg^{0.6}}{16(s-1)(1-p)(2\pi)^{0.2}\kappa^{0.4}\cos\alpha_b^{0.2}} \tag{18}$$

where C_{Ol} = 0.0719 approximately for most types of sand, assuming the effect of α_b is negligible. Monthly distribution of Q_l/C_{ol} is presented in Fig. 12.

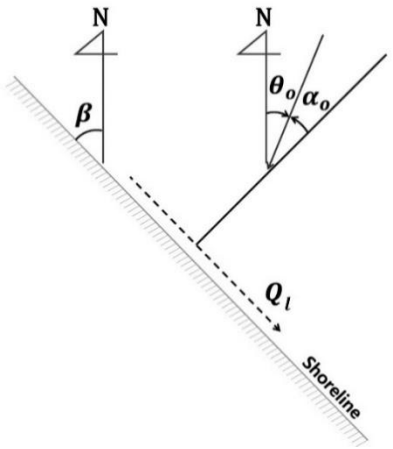

Figure 9: Definition sketch showing deepwater wave angle α_O and others for calculating LST rate in this study.

The long-term shoreline change is calculated using one-line model (Pelnard-Considère, 1956), by considering the difference in the LST along the coast within the active zone between the berm and the depth of closure,

$$\frac{\partial x}{\partial t} + \frac{1}{(h_B + h_C)}\left(\frac{\partial Q_l}{\partial y} - q\right) = 0 \tag{19}$$

where (x, y) are the Cartesian coordinates with x-axis positive pointing seaward, y-axis alongshore and the origin is at the MSL, and h_B and h_C are the berm height and closure depth, respectively. Q_l is the LST rate calculated by the CERC formula (Shore Protection Manual, 1984), and q represents the cross-shore sediment transport per unit width of the shoreline (Lee and Hsu, 2018). An alternative expression for the LST rate, similar to Eq. (17), is given by

$$Q_l = CH_b^{5/2}\sin 2\alpha_m \tag{20}$$

where α_m is the wave angle within the diffracted zone (Lim et al., 2021). However, nearshore currents within the diffraction zone is assumed to be in non-existent, when SEP is reached for the eroded shoreline planform. In the numerical calculations, the quantity of the LST at each grid is calculated or assigned. For example, $Q_l = 0$ is used for the eroding shoreline along the boundary of the groin.

3. Wave and shoreline data

Jeongdongjin Beach (Fig. 1) in Gangwon-do, South Korea, is a littoral cell about 850 m long bounded between two groins – a cluster of pillar rocks behaving like a natural groin in the north end and a land-based artificial structure in the south. Wave data and sediment LST rate required for calculating the spatial and temporal location of the downdrift control point (i.e., x_c in Eq. 4) and maximum indentation point (i.e., x_E and y_E in Eq. 10) can be obtained from analyzing NOAA's wave data.

3.1 NOAA wave data (1979 – 2018)

The European Center for Medium-Range Weather Forecasts and the National Centers for Environmental Prediction (NCEP) under the National Oceanic and Atmospheric Administration (NOAA) in the United States have provided long-term wave hindcast data since January 1979. Since 2004, NOAA has also operated the Climate Forecast System Reanalysis and Reforecast (CFSRR) activity, which analyzes sea climate using observation data that spanning more than 60 years. Saha et al. (2010, 2014) have verified the applicability of NOAA data by assimilating and verifying CFSRR observation data.

For the wave conditions in the open sea applicable to Jeongdongjin Beach, NOAA wave data between 1979 and 2018 are available within a nearby location (129.5° E, 38.0° N). The wave data are analyzed and the results used to calculate the change of the eroding shoreline curve at downdrift of the natural rocky groin caused by the oblique high waves in the winter. First, the monthly root-mean-square (rms or RMS) wave height ($\bar{H}$) is calculated using Eq. (21),

$$\bar{H} = \sqrt{\frac{\sum_{i=1}^{N} H_i^2}{N}} \tag{21}$$

where N is the total number of wave data. In addition, the mean wave period and direction, $\bar{T}$ and $\bar{\alpha}$ can also be calculated from the wave data. Figure 10 depicts the monthly variations in the RMS wave height, period, and direction of the significant

waves, averaged over every 10-year intervals between1979 and 2018. As shown in this figure, the NE waves in winter (December – February) arrive from N10°E approximately, the ENE waves in summer (June –August) approach from N70°E to the study area, and the local shoreline aligns in NW – SE direction (about N133°E).

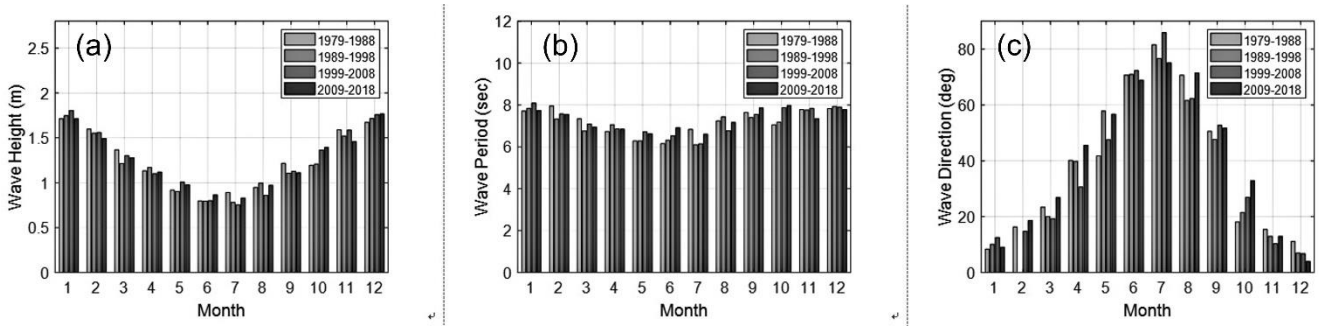

Figure 10: Averaged monthly wave conditions for the study aera: (a) wave height, (b) wave period, and (c) offshore wave direction.

Nearshore wave data were also collected by an AWAC meter (see Fig. 1 for location) at a depth of 32.4 m to the south of Jeongdongjin Beach. From the data recorded over three years (27 September 2013 to 21 November 2016), distribution of the annual mean wave direction is plotted (Fig. 11). The results reveal the prevailing wave direction nearshore was mostly within -15° to +10° from the normal to the local shoreline. However, positive values only are responsible for downdrift erosion of the natural groin at the updrift of Jeongdongjin Beach.

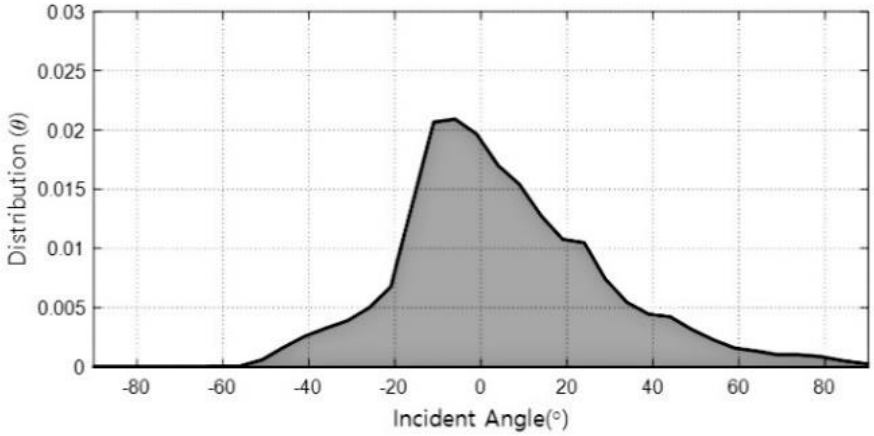

Figure 11: Distribution of the mean wave direction collected by an AWAC meter to the south of Jeongdongjin Beach.

By plotting the monthly wave factor for the LST rate in terms of Q_l/C_{ol}, using NOAA wave data, the results in Fig. 12 reveal a strong seasonal-dependent trend in the direction of the LST, highlighting southward transport in winter months (November to February) and northward in summer (July to September). Thus, downdrift beach erosion with can be expected to reach a maximum around February at the end of winter. However, if the seasonal LST bypasses the beach without being intercepted

by the rocky pillars (Fig. 3) at different water levels and wave conditions, only weak to moderate downdrift erosion could result.

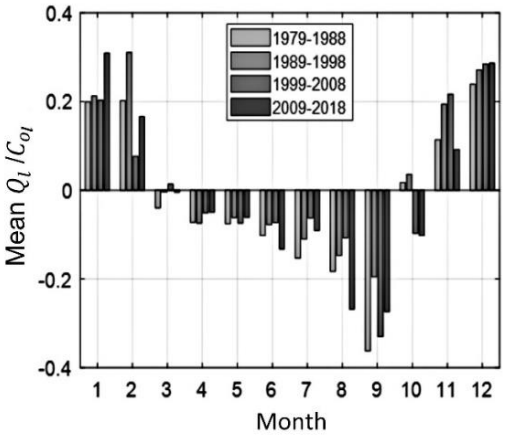

Figure 12: Monthly wave factor of the longshore sediment transport (Q_l/C_{ol}) using NOAA wave data.

Assuming the seabed contours are straight and parallel, then the wave height and wave angle at the breaker are estimated from satisfying linear wave shoaling and refraction relationship ($H/H_0 = K_s K_R$) and spilling wave breaking criteria ($h_b = 1.28\ H_b$) simultaneously (Reeve et al., 2012) from the waves offshore collected in NOAA's wave data. From the results, the monthly average of $H_b^{5/2}$ as a function of the oblique wave direction α_b in 2.5° intervals is graphed (Fig. 13) for waves in winter months (November – February). The wave angle is evaluated based on N38°E as α_b = 0, and the wave height and angle at breaking are calculated by N38°E ± 50° in deep water. The values of $H_b^{5/2}$ where large within -7.5° ~ +12.5°, which imply high waves

in winter that may cause severe beach erosion could arrive from the sector within N38°E – 2.5° to N38°E + 7.5°.

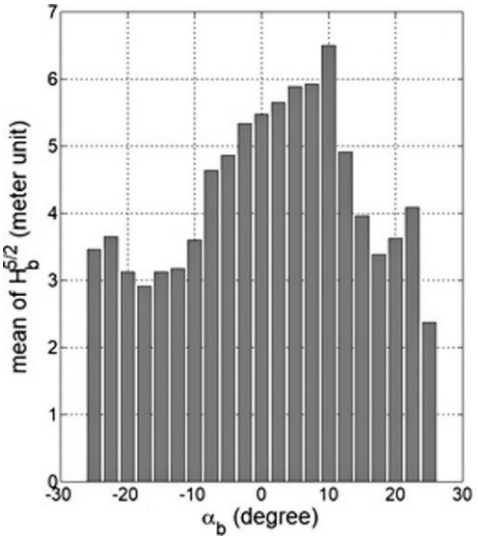

Figure 13: Monthly average of $H_b^{5/2}$ per 2.5° interval of oblique wave angle α_b, obtained from NOAA wave data during winter months.

If an amount of LST (ΔQ) to a beach is accreted at updrift side of a groin on a straight shoreline (Fig. 14), shoreline retreats at downdrift. Once sediment bypassing the tip of the groin, long-term shoreline equilibrium may reach on both sides of the groin. However, during this process of bypassing, the location of A and A' may fluctuates, with the former gradually advancing updrift while the latter slowly shifting downdrift.

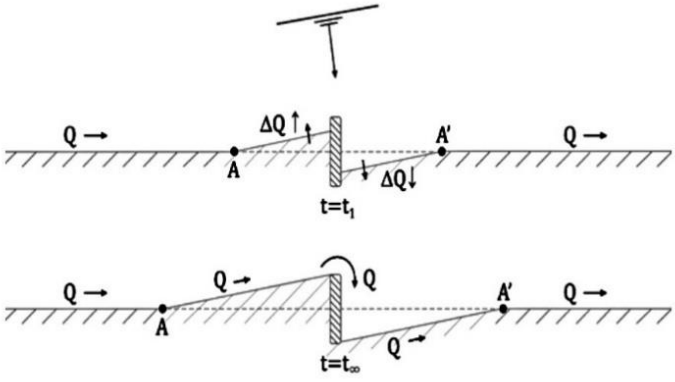

Figure 14: Shoreline change affected by sediment bypassing a groin under oblique waves

3.2 Shoreline video monitoring program

Shoreline monitoring in South Korea have been conducted since 2003, as part of the national Coastal Erosion Survey Project, aiming to promote efficient coastal maintenance in the country via proactive responses based on scientific data collection and analysis. At Jeongdongjin, the video monitoring program has commenced since February 2014, by installing four cameras to cover the shoreline of the beach (Fig. 1).

In this study, the variation of shoreline positions were derived from the time-averaged video images by the geometric transformation equation (Lippmann and Holman, 1989), which transforms the image coordinates to ground coordinates. The video images were taken twice a day during 6 – 30 December in 2015, while the routine one per day operation was continued in the following January and February in 2016 (shown in Fig. 17). However, it should be noted that the location of the critical points on these images might not include that of the instantaneous maximum indentation. Therefore, the actual extent of shoreline retreat may be larger than that presented.

4. Results

In this section, the performance of the analytical model is verified by comparing not only the numerical model but also the shoreline data. Figure 15 compares the temporal variation of the results for analytical and numerical (Lim et al., 2021) results of x_E and y_E at the maximum indentation for τ (= x_c^2/q_b; unit in meter and hour) for three different values of α_b (10º, 15º and 20°) at Jeongdongjin Beach with a natural rocky groin about 80 m long. In the numerical results, the value of y_E (negative) increases (erosion) with time as α_b increases, whilst that of x_E decreases (closer to the boundary from the groin). Similar trend can be found in the analytical results. Moreover, the discrepancies between the numerical and analytical results increases as α_b increases.

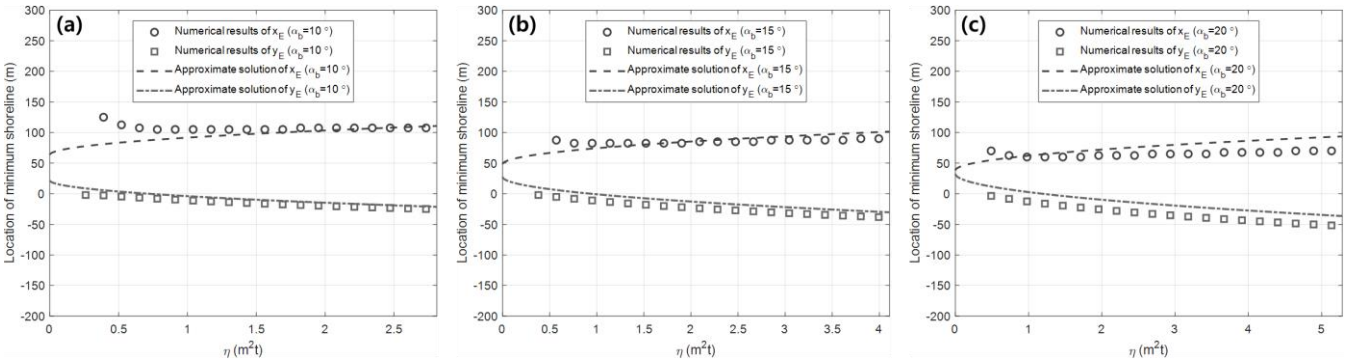

Figure 15: Comparison between analytical and numerical results for breaking wave direction α_b of (a) 10°, (b) 15° and (c) 20°, respectively, for Jeongdongjin Beach.

In addition, the planform of the eroded beach can be simulated using numerical model. First, the results of the numerical model for a series of duration from 6 hours to 4 weeks can be first demonstrated, using α_b = 10° (Fig. 13), are indicated in Fig. 16, using the prototype data for Jeongdongjin Beach (i.e., natural groin with protruding length y_g = 80 m, beach length L = 850 m, winter high waves of 2.11 m, and LST coefficient *C* = 0.0847 in Eq. 16). In this figure, the shoreline near the groin advances seaward within the first six hours, similar to the trend in Fig. 15 (a), prior to being eroded (landward) thereafter. For $\alpha_b = 10^o$, $H_b^{5/2}$ = 6.5 and the maximum erosion length x_c = 425 m (i.e., not exceeding *L*/2), Eq. (10b) gives $y_E = -32.5$ m, which is equivalent to the result of "1 week after" in the numerical model. In addition, the numerical model is also run for other wave angles at breaking (α_b) at 2° intervals, and the results are collectively marked as "analytical results" in Fig. 17.

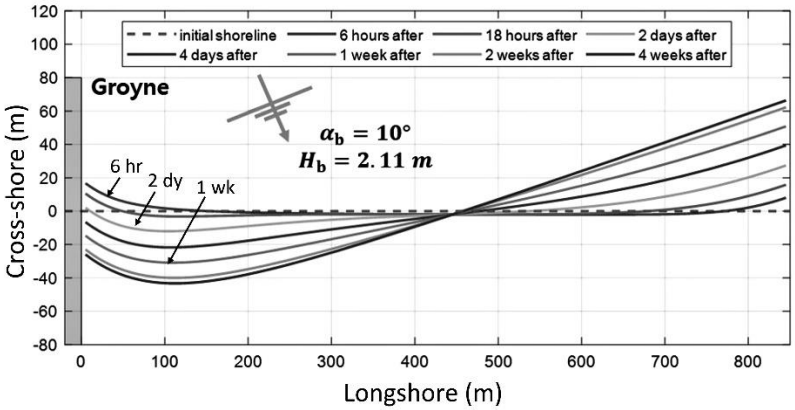

Figure 16: Results of numerical model, showing spatial and temporal variation of the eroding beach planform for α_b= 10°.

The results of analytical method predict the eroding shoreline planform and the maximum indentation point, using the parabolic model with monthly averaged wave conditions from NOAA wave data, whereas that of the video monitoring program reveal the hourly/daily record from the shoreline images corresponding to the instantaneously changing wave conditions. To compare the results coming from these two different sources, the maximum indentation points occurred on the day of video recording is selected. Despite the difference in time scale, Fig. 17 indicate that the results of the analytical prediction are in fair agreement with the video monitoring data. At the duration of 0.6 month (18 days) for waves with α_b = 10° (Fig. 18) obtained from NOAA wave data, numerical model predicts the maximum indentation may reach 40 m for wave actions lasting about 2 weeks (Fig. 16), which also agrees reasonably well with the shoreline video monitoring results (Fig. 17).

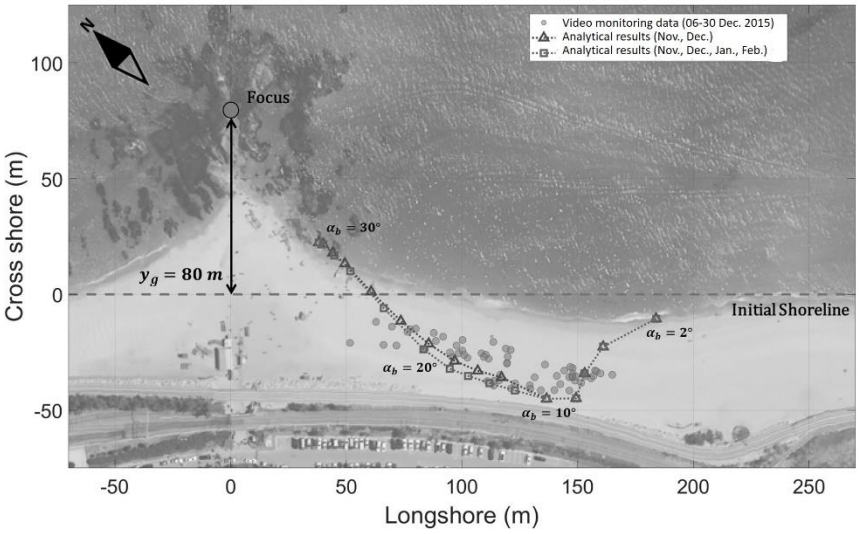

Figure 17: Comparison between video monitoring data and analytical solution.

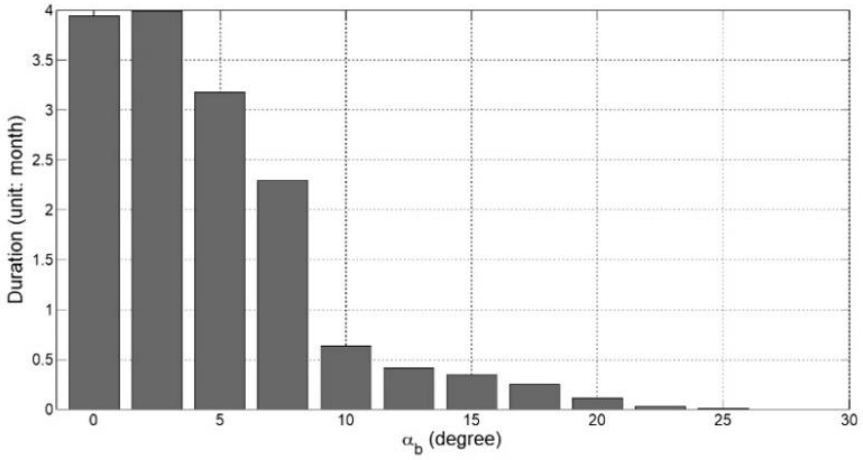

Figure 18: Duration of each oblique wave angle estimated from NOAA data (unit: month).

5. Discussion

(1) This paper deals with downdrift erosion – shoreline retreat hotspot at the downdrift of a natural rocky groin that interrupts the longshore transport during high waves in winter. A predictive for the resultant embayed geometry is developed by deriving mathematical equations from the parabolic bay shape model (Hsu and Evans, 1989). The validity of this analytical model is confirmed for Jeongdongjin Beach on the northeast coast of South Korea by using video monitoring data and one-

line numerical models. When applying this method to other beaches, however, consideration/modification must be taken for locating the downdrift control point, because Jeongdongjin Beach is a littoral cell with 850 m length (Fig. 1), while the others may not. Nevertheless, this robust method can be used a suitable first approximation and will be useful for practical engineers since the approach can be easily applied in case long-term wave data (e.g., NOAA wave data) or shoreline video monitoring results are available.

(2) The method presented in this paper excludes sediment bypassing through the groin at updrift, nor the shoreline retreat due to cross-sediment movement. Therefore, the analytical results for the maximum indentation from Eqs. (10a) and (10b) with LST rate might be underestimated. To include sediment bypassing, the alongshore distance of the downdrift control point (at x_c in Fig. 7) will be limited with breaking wave angle α_b in relation to the protruding length of the groin (Figs. 1 and 17), considering the following relationship,

$$x_c^l = \frac{y_g}{\tan\alpha_b} \tag{22}$$

where superscript *l* denotes limiting value. Here, variables x_c and x_c^l, obtained from Eqs. (10a, 10b) and (23), respectively, are compared in Table 1. If x_c obtained for each α_b is greater than x_c^l for a given y_g, then x_c should be replaced by x_c^l, because bypassing might not occur for α_b between 10° and 17.5°. As shown in Fig. 17, the monitoring data in December 2015 support the analytical solution that uses α_b = 10° for calculating the x_c. In Table 1, η (=$\sqrt{q_b t}$) indicates that there is no effect of protruding length y_g or beach length *L* (= 850 m), because either the LST rate is small, or the wave duration is too short. However, the erosion width may be reduced as bypassing occurs when the protruding length is short. Thus, the limit in x_c in relative to *L* is expected to be within one-half of the beach length (being *L*/2 = 425 m, where *L* = 850 m), which is within the range of beach length covered by the video monitoring equipment.

Table 1: Comparison between the control point locations obtained from NOAA wave data and from Eq. (22).

α_b	2.5	5.0	7.5	10.0	12.5	15.0	17.5	20.0	22.5	25.0	27.5	30
x_c^l(m)	1832	914	608	454	361	299	254	220	193	172	154	139
x_c (m) (Nov., Dec., Jan., Feb.)	1570	1426	1209	662	458	374	288	195	92	21	0	0
Constraint*	L	L	L	y_g	y_g	y_g	y_g	η	η	η	η	η
x_c (m) (Nov., Dec.)	1086	993	859	476	325	264	207	137	63	19	0	0
Constraint*	L	L	L	y_g	η	η	η	η	η	η	η	η

* Parameters in the row marked "Constraint*": L for constraint by beach length, η by longshore drift length ($\sqrt{q_b t}$) and y_g by protruding length of groin.

(3) The present method can be used to estimate the eroding shoreline planform for beach nourishment project, especially by comparing the position of the maximum indentation. For example, to mitigate the extent of downdrift erosion caused by winter high waves, engineering options may be considered either by (1) artificially nourishing the beach to advance the shoreline (Fig. 19), or by (2) placing a short groin to promote sediment accretion within the potentially eroding section (Fig. 20). Fig. 19 compares the reduction in potential beach erosion and its maximum depth y_E for uniformly nourishing the beach by 10 m and 20 m, respectively, which renders y_E of −38 m and −30 m, respectively, compared with that without artificial nourishment (y_E = −45 m), under the same wave condition.

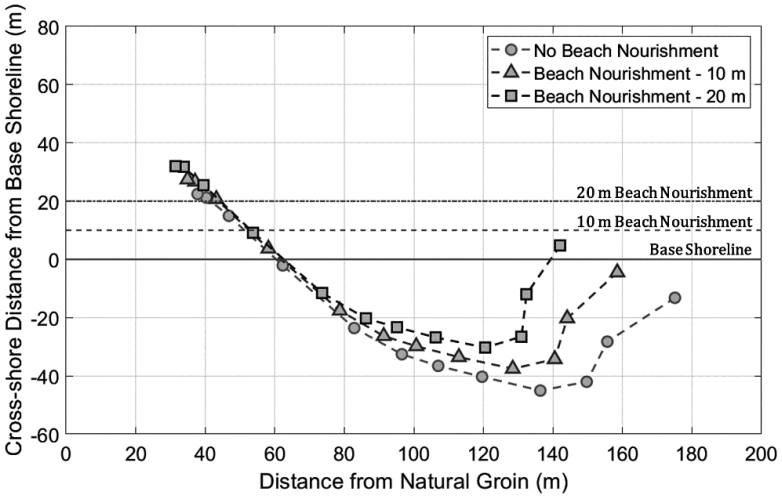

Figure 19: Change of maximum erosion width and indentation induced by beach nourishment of two different widths.

Figure 20 illustrates the temporal shoreline change by placing a short groin at point G where it becomes a new downdrift control point for the potential eroded beach curve. Therefore, the dimension of a potential eroding beach at downdrift of the natural groin can be reduced by sediment accretion fronting the short groin. For example, to limit the maximum erosion of y_E within 20 m for α_b = 10° during winter high waves, a groin may be installed at 327 m from the groin, for which the location can be estimated by Eq. (10b), giving

$$x_c = \frac{(y_g+y_E)\theta}{\cos(\varphi)\, sin\alpha_b} - y_g cot\alpha_b = \frac{(80+20)\times 52.5\pi/180}{cos(47.5)\sin(10)} - 80 \times \cot(10) = 327m \quad (23)$$

in which y_g = 80 m and φ = 47.5° for α_b = 10°.

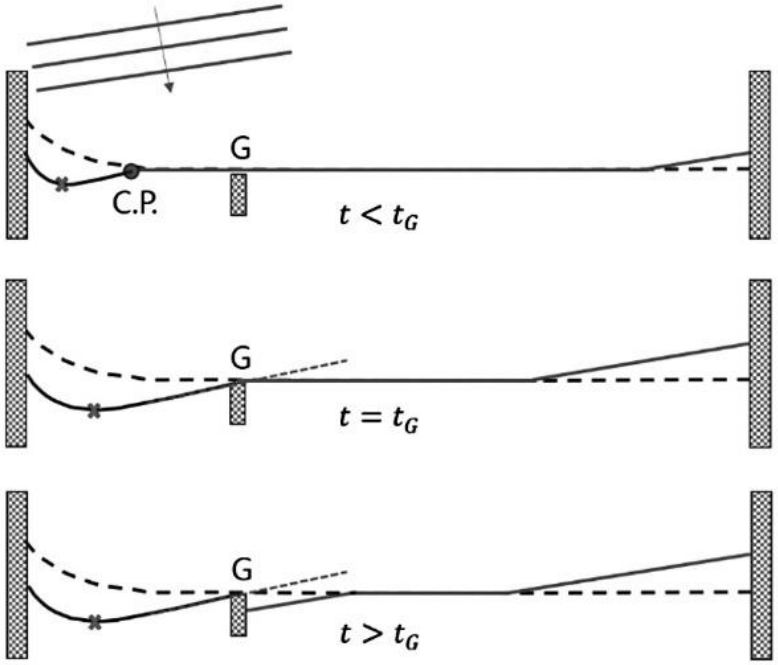

Figure 20: Controlling maximum erosion width by installing a short groin at point G.

6. Conclusions

Downdrift erosion – a phenomenon of localized erosion at the unprotected downdrift end of seawalls or groins, is common, yet rarely taught in the classrooms nor well documented in the literature and coastal engineering journals, leaving the challenging problem for the consulting engineers and coastal managers to deal with (e.g., Headland et al., 2000). During the winter months on the east coast of South Korea, oblique high waves have often generated severe erosion at downdrift stretch of a groin, natural or artificial. For example, beach erosion at downdrift of a cluster of natural pillar rocks at Jeongdongjin had occurred continuously for more than two consecutive month (February – March) in 2016. Video footage revealed that, during this period, the eroded beach remained in a distinctive crenulate shape with maximum indentation about 40 m over some 300 m long. Despite the beach had gradually recovered in the following months (May – June) in calm weather, the erosive scenario had caused disastrous effects not only on the beach environment but also the livelihood of the locals.

The purpose of this study is to introduce an analytical model, simple yet useful, that can help predict the size and shape of the eroded beach of downdrift side, to benefit local coastal managers in maintaining the beaches. By the input of wave conditions (heights and wave angle at breaking) and updrift control point (wave diffraction point) to the mathematical equations derived from the parabolic model for bay beaches in static equilibrium, the maximum indentation and crenulate bay shape can

be predicted. This method is robust and cost effective, comparing to the time consuming and costly physical experiments and the complex numerical models.

Data availability

Not applicable.

Author contributions

Supervision, J.L.L.; Writing—original draft, C.L.; Writing—review & editing, C.L., S.H. and J.L.L.; Data acquisition, C.L. and H.S; Visualization, C.L. and J.L.L.; All authors have read and agreed to the published version of the manuscript.

Competing interests

The authors declare no conflicts of interest.

Acknowledgements

This research is part of a project entitled 'Practical Technologies for Coastal Erosion Control and Countermeasure' supported by the Ministry of Oceans and Fisheries, Korea (20180404).

References

Badiei, P., Kamphuis, J. W. and Hamilton, D. G.: Physical experiments on the effects of groins on shore morphology, in: Proceedings of the Coastal Engineering Conference, 2, 1782–1796, 1994.

Bakker, W.T.: The dynamics of a coast with a groin system, Proc. 11th Inter. Conf. Coastal Eng., ASCE, 492–517, 1968.

Bakker. W.T., Klein Breteler, E.H.J. and Roos, A.: The dynamics of a coast with a groin system, in: Proc. 12th Inter. Conf. Coastal Eng., ASCE, 64, 1001–1020, 1970.

Balaji, R., Kumar, S.S. and Misra, A.: Understanding the effects of seawall construction using a combination of analytical modelling and remote sensing techniques: Case study of Fansa, Gujarat, India, J. Ocean and Climate Systems, 8, 3, 153–160, 2017.

Bayram, A., Larson, M. and Hanson, H.: A new formula for the total longshore sediment transport rate, Coast. Eng., 54, 9, doi:10.1016/j.coastaleng.2007.04.001, 2007.

Dean, R.G. and Dalrymple, R.A.: Coastal Processes with Engineering Applications. Cambridge University Press, Cambridge, UK, 475 pp, 2002.

González, M., Medina, R. and Losada, M.: On the design of beach nourishment projects using static equilibrium concepts: Application to the Spanish coast, Coast. Eng., 57, 2, doi:10.1016/j.coastaleng.2009.10.009, 2010.

Longuet-Higgins, M.S.: Longshore currents generated by obliquely incident sea waves - 1, 2, J Geophys Res, 75, 33, doi:10.1029/jc075i033p06790, 1970.

Hanson, H. and Kraus, N.C.: GENESIS: Generalized Model for Simulating Shoreline Change, Report 1: References manual and users guide, Tech. Report CERC-89-19, U.S. Army Corps of Engineers, Coastal Engineering Research Center, USA, 1989.

Headland, J., Smith, W.G., Kotulak, P. and Alfageme, S.: Coastal protection methods, Ch.8 in Herbich, J.B. (ed), Handbook of Coastal Engineering, McGraw Hill, NY, 8.1–8.66, 2000.

Hsu, J. R. C. and Evans, C.: Parabolic bay shapes and applications, in: Proceedings of the Institution of Civil Engineers, 87, 557-570, doi:10.1680/iicep.1989.3778, 1989.

Hsu, J.R.C., Uda, T. and Silvester, R.: Shoreline protection methods—Japanese experience. in: Herbich, J.B. (ed.), Handbook of Coastal Engineering. McGraw-Hill, New York, 9.1–9.77, 2000.

Inman, D. L. and Nordstrom, C. E.: On the Tectonic and Morphologic Classification of Coasts, J. Geol., 79, 1-21, doi:10.1086/627583, 1971.

Kamphuis, J. W.: Alongshore Sediment Transport Rate, J. Waterw. Port, Coastal, Ocean Eng., 117, 6, doi:10.1061/(asce)0733-950x(1991)117:6(624), 1991.

Kim, D. S. and Lee, G.-R.: Seasonal Changes of Shorelines and Beaches on East Sea Coast, South Korea, J. Korean Geogr. Soc., 50, 2, 2015.

Komar, P.D., Inman D.L.: Longshore sand transport on beaches. J. Geophys. Res., 75, 30, 5914-5927. https://doi.org/10.1029/jc075i030p05914, 1970

Kraus, N.C., McDougal, W.G.: The effects of seawalls on beaches, Part 1: An updated literature review. J. Coastal Research, 12(3), 691–701, 1996

Larson, M., Hanson, H. and Kraus, N. C.: Analytical solutions of the one-line model of shoreline change, Tech. Rep. - US Army Coast. Eng. Res. Cent., 87–15, 1987.

Larson, M., Hanson, H., Kraus, N.C.: Analytical solutions of the one-line model for shoreline change near coastal structures. J. Waterways, Port, Coastal and Ocean Eng., ASCE, 180–191, 1997.

Le Méhauté, B. and Soldate, M.: Mathematical modeling of shoreline evolution, in Proceedings of the Coastal Engineering Conference, 2, 1979.

Lee, J. L. and Hsu, J. R. C.: Numerical simulation of dynamic shoreline changes behind a detached breakwater by using an equilibrium formula, in Proceedings of the International Conference on Offshore Mechanics and Arctic Engineering - OMAE, 7A, V07AT06A036, https://doi.org/10.1115/OMAE2017-62622, 2017.

Lehnfelt, A. and Svendsen, S.V.: Thyboroen channel – difficult coastal protection problem in Denmark. Ingenioeren, 2, 66–74, 1958.

Leont'yev, I. O.: Short-term shoreline changes due to cross-shore structures: A one-line numerical model, Coast. Eng., 31, 59-75, doi:10.1016/S0378-3839(96)00052-X, 1997.

Lim, C., Lee, J. and Lee, J. L.: Simulation of bay-shaped shorelines after the construction of large-scale structures by using a parabolic bay shape equation, J. Mar. Sci. Eng., 9, 1, doi:10.3390/jmse9010043, 2021.

Lim, C. B., Lee, J. L. and Kim, I. H.: Performance test of parabolic equilibrium shoreline formula by using wave data observed in east sea of korea, J. Coast. Res. SI, 91, doi:10.2112/SI91-021.1, 2019.

Lippmann, T. C. and Holman, R. A.: Quantification of sand bar morphology: a video technique based on wave dissipation, J. Geophys. Res., 94, C1, doi:10.1029/JC094iC01p00995, 1989.

Longuet-Higgins, M.S.: Longshore currents generated by obliquely incident sea waves, 1. J. Geophys. Res. 75, 6778–6789, 1970a.

Longuet-Higgins, M.S.: Longshore currents generated by obliquely incident sea waves, 2. J. Geophys. Res. 75, 6790–6801, 1970b.

Magoon, O.T., Edge, B.L.: Stabilization of shoreline by use of artificial headlands and enclosed beaches. Proc. Coastal Zone'78, ASCE, v.2, 1367–1370, 1978.

Moreno, L. J. and Kraus, N. C.: Equilibrium Shape of Headland-Bay Beaches for Engineering Design, in: Proceedings of the Coastal Sediments '99, 860, 1999.

Ozasa, H. and Brampton, A. H.: Mathematical modelling of beaches backed by seawalls, Coast. Eng., 4, 47-63, doi:10.1016/0378-3839(80)90005-8, 1980.

Pelnard-Considère, R.: Essai de theorie de l'evolution des formes de rivage en plages de sable et de galets, Journées de L'hydraulique, 4, 1, 289-298, 1956.

Price, W.A., Tomlinson, K.W.: The effect of groynes on eroded beaches. Proc. 12th Inter. Conf. Coastal Eng., ASCE, Ch. 67, pp. 1053–1058, 1970.

Reeve, D., Chadwick, A., Fleming, C.: Coastal Engineering: Processes, Theory and Design Practice, 2nd Ed. Spon Press, Taylors & Francis, London, 514 pp, 2012.

Saha, S., Moorthi, S., Pan, H. L., Wu, X., Wang, J., Nadiga, S., Tripp, P., Kistler, R., Woollen, J., Behringer, D., Liu, H., Stokes, D., Grumbine, R., Gayno, G., Wang, J., Hou, Y. T., Chuang, H. Y., Juang, H. M. H., Sela, J., Iredell, M., Treadon, R., Kleist, D., Van Delst, P., Keyser, D., Derber, J., Ek, M., Meng, J., Wei, H., Yang, R., Lord, S., Van Den Dool, H., Kumar, A.,

Wang, W., Long, C., Chelliah, M., Xue, Y., Huang, B., Schemm, J. K., Ebisuzaki, W., Lin, R., Xie, P., Chen, M., Zhou, S., Higgins, W., Zou, C. Z., Liu, Q., Chen, Y., Han, Y., Cucurull, L., Reynolds, R. W., Rutledge, G. and Goldberg, M.: The NCEP climate forecast system reanalysis, Bull. Am. Meteorol. Soc., 91, 8, doi:10.1175/2010BAMS3001.1, 2010.

Saha, S., Moorthi, S., Wu, X., Wang, J., Nadiga, S., Tripp, P., Behringer, D., Hou, Y. T., Chuang, H. Y., Iredell, M., Ek, M., Meng, J., Yang, R., Mendez, M. P., Van Den Dool, H., Zhang, Q., Wang, W., Chen, M. and Becker, E.: The NCEP climate forecast system version 2, J. Clim., 27, 6, doi:10.1175/JCLI-D-12-00823.1, 2014.

Silvester, R. and Hsu, J. R. C.: Coastal stabilization: innovative concepts, Coast. Stab. Innov. concepts, 578, doi:10.1016/0037-0738(93)90155-x, 1993.

USACE (U.S. Army Corps of Engineers): Shore protection manual. Department of the Army, U.S. Corps of Engineers, Washington, D.C. 20314, 1984

USACE: Coastal Engineering Manual. US Army Corps of Engineers: Washington, DC, USA. http://chl.erdc.usace.army.mil/chl.aspx?p_s&a_articles;104 (accessed on 30 Aril 2002) , 2002.

Walton, T. L. and Chiu, T. Y.: A review of analytical techniques to solve the sand transport equation and some simplified solutions. in: Proceedings of the Coastal Structures ’79, ASCE, 809–837, 1979.

Wang, P. and Kraus, N. C.: Movable-Bed Model Investigation of Groin Notching, Source J. Coast. Res. J. Coast. Res. SI, 33, 342-368, 2004.

Yasso, W. E.: Plan Geometry of Headland-Bay Beaches, J. Geol., 73, 5, doi:10.1086/627111, 1965.